ACS Sustainable Chemistry & Engineering

Research Article

pubs.acs.org/journal/ascecg

Self-Assembled Three-Dimensional Graphene-Based Aerogel with Embedded Multifarious Functional Nanoparticles and Its Excellent Photoelectrochemical Activities

Weijia Han,† Long Ren,† Lunjun Gong, Xiang Qi,* Yundan Liu, Liwen Yang, Xiaolin Wei, and Jianxin Zhong

Laboratory for Quantum Engineering and Micro-Nano Energy Technology and Faculty of Materials and Optoelectronic Physics, Xiangtan University, Hunan 411105, P. R. China

Supporting Information

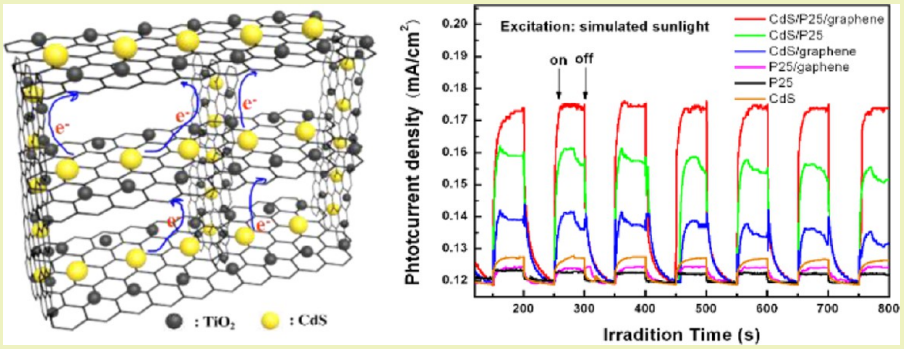

ABSTRACT: Here, a graphene-based aerogel embedded with two types of functional nanoparticles shaped in a three-dimensional (3D) cylindrical architecture was prepared by a facile one-pot hydrothermal process. During the hydrothermal reaction, the uniformly dispersed TiO_2 (P25) and CdS nanoparticles were loaded on the graphene sheets, and the resulting composites were self-assembled into a 3D interconnected network. It is shown that the graphene-based hydrogel and aerogel are appropriate and robust hosts for anchoring different functional nanostructured particles. The outstanding synergistic effect of this ternary graphene-based nanocomposite aerogel is also proved by the excellent photoelectrochemical activity of the as-prepared novel nanocomposite (CdS/P25/graphene) aerogel. As a new photocatalyst, the CdS/P25/graphene aerogel exhibits enhanced light absorption, improved photocurrent, extremely efficient charge separation properties, and superior durability. These excellent properties indicate that the as-prepared CdS/P25/graphene aerogel may have a great potential application in photoelectrochemical hydrogen production from water reduction under sunlight. More importantly, in this study, a significant and pragmatic consideration of integrating multifarious functional nanoobjects into the 3D graphene-based aerogel has been clearly proposed. This could provide new insights into the preparation of functional nanocomposites and facilitate their applications in related areas.

KEYWORDS: *Graphene, Aerogel, Ternary nanocomposites, Photocatalyst*

INTRODUCTION

Compared with other carbon materials, graphene is a more attractive supporting material for nanoobject loading due to its high surface area, fast two-dimensional electron-transfer kinetics, good mechanical strength, and high stability.[1,2] More importantly, the abundant functional groups on the surfaces of the graphene oxide precursor provide many favorable sites for anchoring the functional nanocomponents.[3] The promising properties combined the advantages of both graphene and nanoparticles make graphene-based nanocomposites ideal candidates for incorporation into a variety of functional materials and application in a wide range of fields, such as photocatalysis, electrochemistry, electronic and photonic devices, energy, and sensors.[4−7] However, the close stacking of graphene sheets by forming irreversible agglomerates during the assembling and drying process limits the accessible surface areas for electrolyte ion infiltration and thus leads to a huge loss of electro-active sites.[8,9] These issues may be addressed by the recently developed graphene aerogel, which consists of a unique three-dimensional (3D) porous graphene skeleton. Professor Shi and his team have first reported a facile hydrothermal process to prepare a unique cylindrical graphene hydrogel and aerogel,[10] and it was noted that the graphene aerogel is an ideal prototype for the maximization of accessible surface areas and development of high-performance photocatalyst and electrochemical devices.[11]

Received: October 11, 2013
Revised: December 9, 2013
Published: December 23, 2013

Inspired by recent studies on various routes of preparing the 3D graphene hydrogel/aerogel, it is possible to prepare nanocomposites of 3D graphene-embedded nanoparticles during a reduction and self-assembly process.[12−16] The nanoparticles can be captured into the graphene network during network formation if the nanoparticles are dispersed homogeneously in the graphene oxide (GO) aqueous suspension.[17] Yan has interestingly compared this phenomenon to a fishing process with fishing net, where the fish are the nanoparticles and the fishing net is composed of graphene/graphene oxide nanosheets that can be self-assembled together to form a network during reduction.[18] It indicates the possibility and commonness for most types of nanoparticles to embed in the network structure of the graphene aerogel.

Many graphene-based nanocomposite hydrogels and aerogels have been recently prepared for various applications, such as catalysis and energy storage.[19,20] The hydrogels and aerogels often exhibit enhanced performance benefited from the 3D interconnected network and macroporosity of the architecture that facilitates the charge transfer and improves the specific surface area. However, most of these composites consist of graphene and a single type of nanomaterial; loading multifarious types of nanomaterials on a graphene sheet and assembling them as a 3D aerogel has rarely been reported. According to the former research about a unique ternary graphene-based nanomaterial,[21−23] we found the performance of the as-prepared ternary sample is a significantly enhanced benefit from the advantages of each component and the synergistic interaction among the three components.

On account of the advantages of both the ternary graphene-based nanomaterial and graphene-based aerogel, in this paper, we successfully load two types of nanoparticles (CdS and Degussa P25) onto the graphene nanosheets and form 3D graphene-based nanocomposite aerogels. TiO_2 is the most common photocatalytic materials.[24−26] The couplings of the graphene with TiO_2 and CdS with TiO_2 have been reported to improve the photoelectrochemical catalytic performance owing to improved separation of photogenerated electron−hole pairs with the assistance of graphene and extended absorption edge up to the visible region with the assistance of CdS, respectively.[27−31] Here, the as-prepared CdS/P25/graphene hybrid shows an interconnected macroporous framework of graphene sheets with uniform deposition of a wide band gap catalyst TiO_2 unit and low band gap semiconductor CdS unit. Besides the advantages of each part in the ternary aerogel, there would be some synergistic interactions among the three components such as the transports of the carriers through the three components and the shift of the Fermi energy level. Consequently, the ternary aerogel possesses novel physicochemical properties and exhibits enhanced light absorption, improved photocurrent, extremely efficient charge separation properties, and superior durability as a catalyst. These unique properties demonstrate the potential of 3D CdS/P25/graphene aerogel as an attractive hybrid photocatalyst for photoelectrochemical H_2 production, and it will be a proof of concept for developing and improving practical applications of nanocomposites by integrating multifarious functional nanoobjects into the 3D graphene-based aerogel.

EXPERIMENTAL MATERIALS AND METHODS

Materials. Graphite flakes were purchased from Sinopharm Chemical Reagent Co., Ltd. The TiO_2 nanopowders (Degussa P25 grade) were purchased from Degussa, and CdS nanoparticles (99.999%) were purchased from Aladdin Chemistry Co., Ltd. All the other reagents were of analytical purity and were used as received from Shanghai Chemical Company and without further purification.

Synthesis of Catalyst. First, graphene oxide was synthesized from graphite powder by the modified Hummer's method[32] using a mixture of H_2SO_4, $NaNO_3$, and $KMnO_4$. A previous graphite oxidation procedure with H_2SO_4, $K_2S_2O_8$, and P_2O_5 was carried out before the synthesis of GO. The CdS/P25/graphene aerogel was obtained via a hydrothermal-method based on Shi's work[10] with modifications. In detail, 30 mL of GO brown colloidal dispersion (3 mg/mL) was prepared by ultrasonic treatment for 1 h, and then 0.2 g of TiO_2 (P25) and 0.1 g of CdS were added into the obtained GO colloidal dispersion and stirred for another 2 h to get a homogeneous suspension. The suspension was then placed in a 50 mL Teflon-sealed autoclave and maintained at 180 °C for 12 h to form a network during the reduction of GO and to embed the nanoparticles of P25 and CdS on the graphene support. Finally, after cooling to room temperature, a columnar hydrogel of 3D graphene loaded with P25 and CdS nanoparticles was obtained. The free-standing CdS/P25/graphene hydrogel was taken out, washed with distilled water, and freeze-dried into an aerogel overnight for further use. For comparison, CdS/P25/graphene aerogels with different weight ratios, nonporous graphene/P25/CdS, CdS/P25 composites, CdS/graphene aerogel, P25/graphene aerogel, pure graphene aerogel, pure P25, and pure CdS have been also prepared. Details of the preparation of the comparison groups are given in the Supporting Information.

Characterization. The crystal structures of the as-prepared samples were determined by X-ray diffraction (XRD) using Cu Kα radiation. The morphologies and microstructures of the samples were characterized using scanning electron microscopy (SEM, JEOL, JSM 6360) and transmission electron microscopy (TEM, JEM2100) with an energy dispersive spectroscope (EDS). Raman spectra were collected by using the Renishaw InVia Raman microscope, excited at room temperature with an excitation laser wavelength of 532 nm. The UV−vis absorption spectra were measured under the diffuse reflection mode using a Shimadzu 2550 UV−visible spectrometer equipped with an integrating sphere (ISR-2200, Shimadzu). Fine $BaSO_4$ powder was used as a standard for baseline measurements, and the spectra of the samples with the same mass in powder form were recorded in a range of 200−800 nm.s

Photoelectrochemical (PEC) H_2 Generation. The experiments of H_2 generation from water were implemented in a square box with different photoanodes (CdS/P25/graphene aerogels, nonporous graphene/P25/CdS, CdS/P25, CdS/graphene, P25/graphene, pure P25, and pure CdS) and cathode (Pt flake). A Ag/AgCl electrode was used as the reference electrode. A detailed description of the procedures for preparing the working electrodes is given in the Supporting Information. The box was provided with a 60 mm ×100 mm quartz window for light incidence. The electrolyte was a mixture of an aqueous solution of 0.24 M Na_2S and 0.35 M Na_2SO_3, where Na_2S acted as a hole scavenger and was oxidized into S_2^{2-} to prevent the photocorrosion of CdS,[30] and the electrolyte solution was first degassed by passing a flow of purified argon gas for at least 20 min. A CHI660D (ChenHua, China) electrochemistry workstation was used to control the potential and record the photocurrent generated. A 150 W high-pressure xenon lamp (CHF-XM150W) with an AM 1.5 filter was placed 10 cm away from the reaction vessel, which was used to provide simulated sunlight. The illumination intensity on the photoanode was fixed at 100 mW/cm^2. The linear sweep voltammograms of the different samples under light illumination were recorded at a scan rate of 10 mV/s. All the experiments were carried out at the same condition. The charge transfer resistance was determined by electrochemical impedance spectroscopy (EIS), which was done at open circuit potential under similar conditions as described above for PEC tests. The amplitude of the sinusoidal wave was 10 mV, and the frequency range examined was 100 kHz to 0.1 Hz.

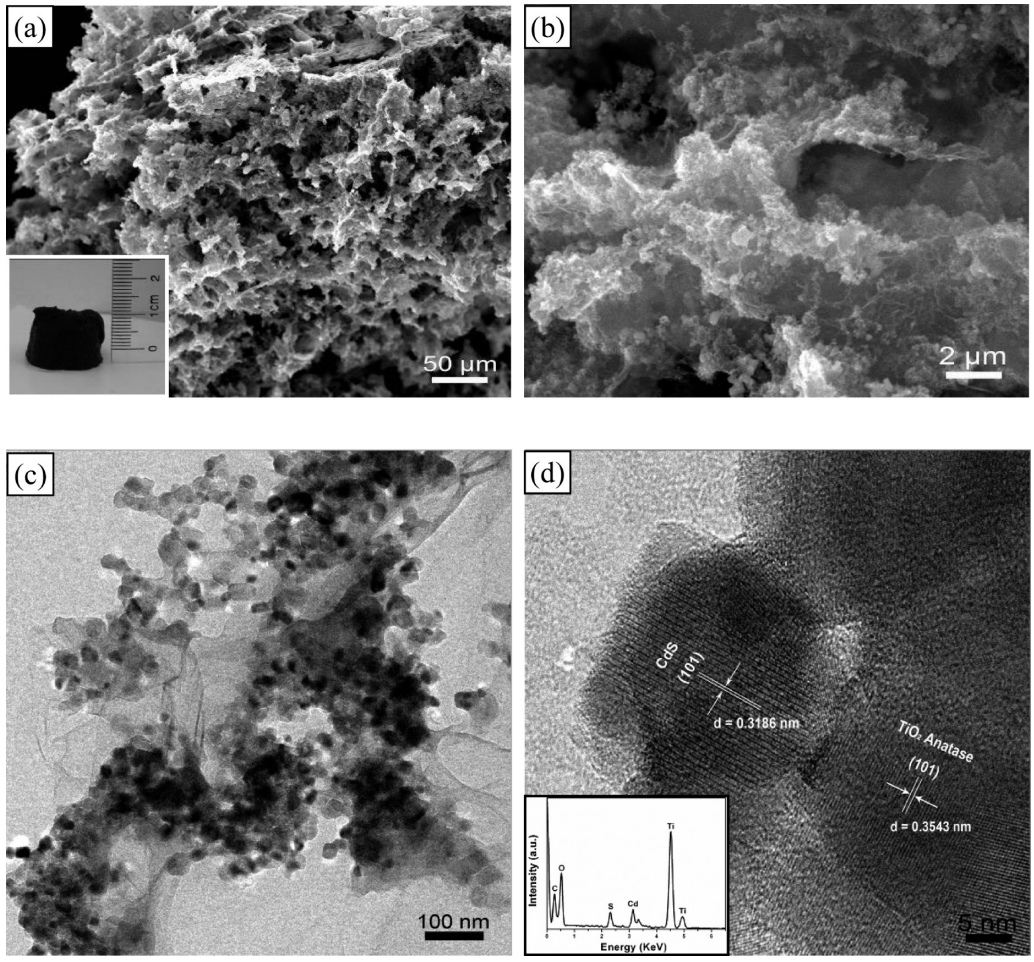

Figure 1. (a, b) SEM images of the as-prepared CdS/P25/graphene aerogel. Inset image is the digital photo of the free-standing CdS/P25/graphene aerogel. (c, d) TEM images and EDS (insert) pattern of the as-prepared CdS/P25/graphene aerogel.

RESULTS AND DISCUSSION

Morphology and Microstructure Characterizations. After the hydrothermal reaction, the ternary CdS/P25/graphene hydrogel was successfully prepared, and the ternary aerogel, which is shown in the inset the digital image of Figure 1(a), would be obtained after a freeze-drying process. The morphologies and microstructures of the obtained ternary CdS/P25/graphene aerogel are characterized by SEM and TEM. As shown in Figure 1 (a), the cross-section SEM images of the ternary aerogel were conducted to reveal the internal characteristics of the sample. The as-obtained CdS/P25/graphene aerogel exhibits a well-defined and interconnected 3D porous network structure with several micrometers of interconnected pores. From the highly magnified SEM image (Figure 1(b)) and TEM image (Figure 1(c)), it is easy to observe that the CdS and TiO_2 nanoparticles are densely embedded into the graphene aerogel network, and unapparent aggregated nanoparticles can be clearly observed anchoring on the graphene plane supports. Moreover, the graphene sheets are rather thin and wrinkled, indicating the efficient self-assembly of graphene sheets. In the HRTEM image (Figure 1(d)) taken from a small region shown in Figure 1(c), one can observe several particles connected with each other. The lattice fringes with a *d* spacing of 0.354 nm can be assigned to the (101) lattice planes of the anatase TiO_2 phase, and the spacing of 0.318 nm can be ascribed to the (101) crystal face of greenockite CdS. The coexistence and connection of the embedded CdS and TiO_2 nanoparticles are confirmed. The elemental mapping (inset in Figure 1(d)) of the ternary aerogel obtained by EDS also indicates that the atomic ratios of the elements are close to their feeding molar ratios. What we described above suggests that these two functional nanoparticles are successfully loaded on the graphene sheets, and the resulting composites are self-assembled into a 3D interconnected network during the hydrothermal treatment. It has been reported that such a 3D graphene-based geometric framework of embedded nanoparticles can enhance its interface contact and suppress the dissolution and agglomeration of nanoparticles, while improving the photoelectrochemical activity and stability of the hybrids.[19] Therefore, a 3D graphene-based aerogel embedded with two types of photocatalyst nanoparticles was successfully achieved.

Figure 2 shows the powder X-ray diffraction patterns of the as-prepared CdS/P25/graphene aerogel as well as pristine P25 and CdS nanoparticles. The XRD pattern of the CdS/P25/graphene aerogel indicates that the ternary sample is well crystallized. Meanwhile, it is easily found that all the diffraction peaks for the pristine cadmium sulfide sample could be well indexed to CdS (JCPDS file no. 41-1049) and that pristine P25 is well indexed to anatase TiO_2 (JCPDS file no. 21-1272) and rutile TiO_2 (JCPDS file no. 21-1276). The ternary aerogel also exhibits all the XRD peaks for CdS and P25, which agrees well with the TEM characterization, but the signal for the carbon

dx.doi.org/10.1021/sc400417u | ACS Sustainable Chem. Eng. 2014, 2, 741−748

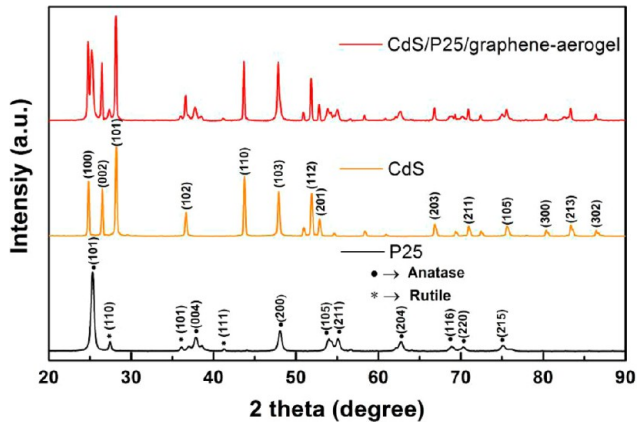

Figure 2. XRD patterns of P25, CdS, and CdS/P25/graphene aerogel.

species was not observed, which might be due to the relatively low diffraction intensity of graphene. Therefore, it is believed that the inherent structures of the raw materials do not change during the hydrothermal treatment.

In order to further clarify the characterizations of the ternary aerogel, Raman spectroscopy analysis was carried out. Figure 3

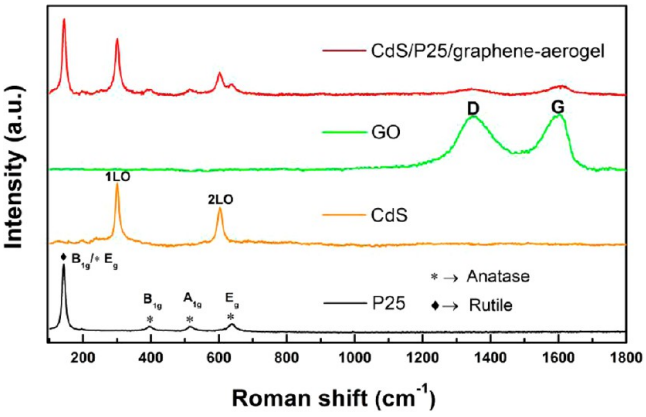

Figure 3. Raman spectra of pristine graphene oxide, P25, CdS, and CdS/P25/graphene aerogel.

illustrates the Raman spectra of GO, CdS, P25, and CdS/P25/graphene aerogel, respectively. The peaks observed at 305 and 602 cm^{-1} in the Raman spectrum of nanostructured CdS can be indexed to the A1 LO and 2LO mode of CdS,[33] respectively. For the pristine P25 sample, the Raman band at 143 cm^{-1} is very intense and sharp, which can be mainly attributed to the B_{1g} mode in rutile as well as the E_g mode at 144 cm^{-1} in anatase. In addition, the Raman peaks at 396, 513, and 639 cm^{-1} are assigned to the B_{1g}, A_{1g}, and E_g modes of anatase,[34] respectively. The characteristic peaks of CdS and P25 were detected simultaneously in the ternary composites, confirming that the hydrothermal treatment does not destroy the structure of CdS and P25, which is in good agreement with previous XRD results. Moreover, the major peaks of GO are the G-band at 1603 cm^{-1} and D-band at 1358 cm^{-1}. The G-band (graphite carbon band) originates from the in-plane vibration of sp2 carbon atoms, and the D-band (disordered carbon band) is attributed to the first-order zone boundary phonons, which is absent from defect-free graphene but exists in defect-contained graphene.[35] After hydrothermal treatment, the D-band and G-band are still present at 1611 and 1338 cm^{-1}, respectively. However, the D/G intensity ratio of the CdS/P25/graphene sample was decreased compared with the GO precursor, which is proposed to be a result of the reduction of GO during hydrothermal treatment.[36] The integrity of the components and unique structure of the ternary composite aerogels make us strongly believe that it would be an excellent photocatalyst for photoelectrochemical H_2 production with outstanding photoelectrochemical activities and stability.

UV−Vis Diffuse Reflectance Spectra (DRS). To gain insight into the suitability of the CdS/P25/graphene aerogel for photoelectrochemical applications, UV−vis diffuse reflectance spectra (DRS) were used to determine the optical properties of the samples. Figure 4 shows the DRS spectra of CdS/P25/

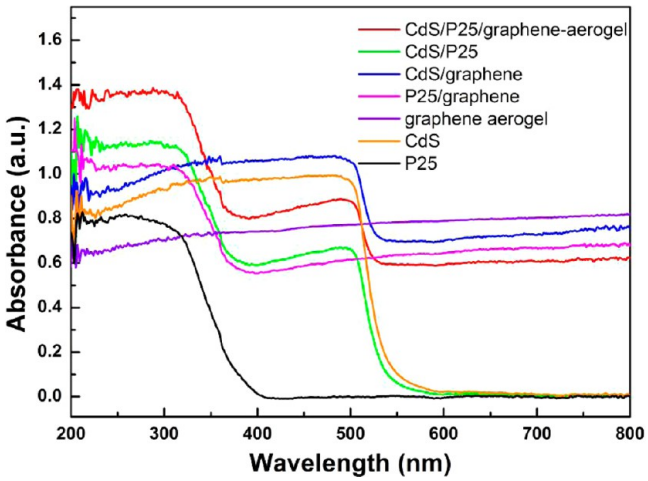

Figure 4. UV−vis diffuse reflectance spectra (DRS) of CdS/P25/graphene aerogel, CdS/P25, CdS/graphene aerogel, P25/graphene aerogel, pure graphene aerogel, CdS nanoparticles, and P25 nanoparticles.

graphene aerogel, CdS/P25, P25/graphene aerogel, CdS/graphene aerogel, pure graphene aerogel, pure CdS, and P25, respectively. Comparing with the DRS spectra of composites and isolated P25, it is easily observed that the introduction of CdS has a favorable impact on the absorption intensity of the samples. Moreover, the characteristic absorption sharp edge of the ternary CdS/P25/graphene aerogel undergoes a red shift compared with binary composites (CdS/P25 and P25/graphene aerogel) and pure monosemiconductors (CdS and P25), which may be due to the synergy effects of three different units in the ternary aerogel, similar with the band gap-narrowing phenomenon of TiO_2 and CdS after the introduction of graphene reported in previous work.[37] The absorption capability in the visible region of the ternary CdS/P25/graphene aerogel is almost the same as that of the CdS/graphene aerogel, which indicates that the addition of the wide gap semiconductor TiO_2 does not obstruct the light absorption. In this case, the enhanced absorption ability of ternary aerogel is mainly proposed to be attributed to the introduction of the third component CdS and the synergistic effects among the three components. Moreover, the DRS spectra of the pure graphene aerogel shows a broad absorption from 200 to 800 nm, which implies that such a 3D graphene-interconnected network structure also plays an effective role to improve the absorption range of the ternary aerogel.

Photoelectrochemical Measurements. It is well known that the photoactivity for hydrogen production increases

remarkably in nanomaterials with the excellent interparticle electron transfer process.[38] Because of the favorable positions of the conduction bands in the binary semiconductor composites, the photogenerated electron could transfer from one semiconductor to the other more easily, resulting in efficient electron transfer for the reduction of the H^+ ion. In this article, ternary CdS/P25/graphene aerogel is tested for solar H_2 generation from water. The CdS/P25/graphene aerogel electrode is used as a photoanode (exposed area 0.7 cm^2) in the PEC cell to evaluate its photoactivity to generate H_2 from water in a sulfide−sulfite (S^{2-}/SO_3^{2-}) electrolyte under simulated solar light illumination (100 mW/cm^2). The PEC tests are carried out using Pt as the cathode and Ag/AgCl as the reference electrode. The PEC activities of the as-prepared photoanodes under illumination conditions are presented in Figure 5, which describe the generation of H_2 through various photoanode PEC reactions and their corresponding photocurrent. According to the Faraday's law, the amount of H_2 evolved is found equivalent to the amount of current generated in the PEC cell.[39] This verifies that the measured current in the system is contributed to H_2 evolution and not the photocorrosion of the catalyst. All the results presented here are in the form of photocurrent density. Before comparing with other type samples, the performance of the proposed composite has been optimized by modulating their compositions. The CdS/P25/graphene aerogel sample with a weight ratio of raw material (90 mg of GO in 30 mL of aqueous solution with the addition of 0.2g of TiO_2/0.1g CdS) has been selected as the optimization, and a maximum photocurrent density of 15.2 mA/cm^2 is obtained at 0.48 V from this ternary aerogel photoanode. The related data are given in the Supporting Information. Please note that in the main part of this paper this optimization is used as the standard sample (marked as CdS/P25/graphene aerogel) for comparing with the other types of samples. Controlled experiments are carried out for further evaluating the performance of the proposed ternary aerogel, which are depicted in Figure 5. The photoactivity of the ternary aerogel is observed to be 3−4 fold more compared to the P25 (4.21 mA/cm^2) and CdS (5.89 mA/cm^2) photoanodes.

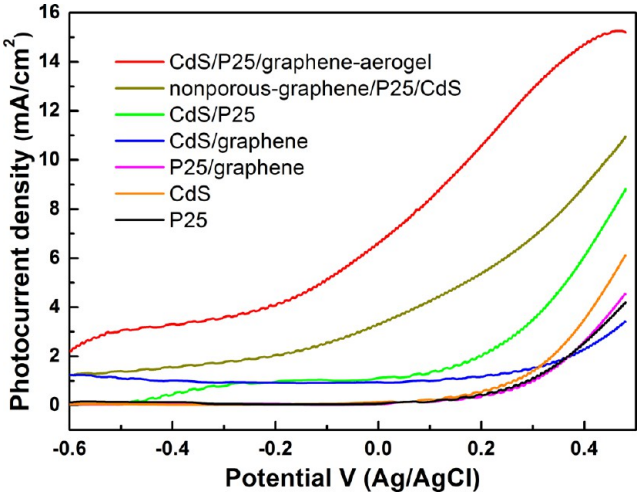

Figure 5. Photocurrent obtained from CdS/P25/graphene aerogel, nonporous graphene/P25/CdS nanocomposite, CdS/P25, CdS/graphene aerogel, P25/graphene aerogel, CdS nanoparticles, and P25 nanoparticles in a sulfide−sulfite electrolyte and under irradiation of simulated sunlight.

Compared to pure P25 and CdS monosemiconductors, the binary hybrids show enhanced activity; thereinto, the values of the maximum photocurrent density of CdS/P25, P25/graphene aerogel, and CdS/graphene aerogel are 8.8, 4.51, and 6.52 mA/cm^2, respectively. However, all of these values for binary hybrids are much less than those for the CdS/P25/graphene aerogel and even the nonporous graphene/P25/CdS nanocomposite, indicating that the synergy of the ternary graphene-based nanocomposites can significantly improve photocatalytic activity, and a further increase in photocatalytic activity would be achieved in the presence of a 3D graphene-interconnected network structure.

As we know, the interface charge separation efficiency of photogenerated electrons and holes is a vital factor for photocatalytic activity. It can be investigated by the typical electrochemical impedance spectra. Figure 6 shows the EIS Nynquist plots of various electrodes. The radius of the arc on the EIS spectra mirrors the interface layer resistance occurring at the surface of the electrode, and the smaller arc radius infers the higher efficiency of charge transfer.[40,31] It is observed that the arc radius of the CdS/P25/graphene aerogel is the smallest one. It is also noted that the internal resistance of the binary CdS/P25 semiconductor composites is much lower than that of the pure P25 and CdS monosemiconductors, which can be contributed to the interparticle electron transfer process, consistent with the DRS results. Compared with the plots of electrodes with and without graphene, it is easy to determine the the presence of graphene can be a benefit to the transport of photoinduced electrons for excellent conductivity of graphene.[22,27] Moreover, the 3D porous architecture is regarded as an important factor to improve the charge transfer in aerogel with the evidence of the difference between the CdS/P25/graphene aerogel and nonporous graphene/P25/CdS nanocomposites.[20,41] The above EIS results and discussions suggest that a 3D graphene-based aerogel with embedded multifarious functional nanoparticles can dramatically enhance the separation and transfer efficiency of photogenerated electron−holes pairs through an interfacial interaction among P25, CdS, and graphene.

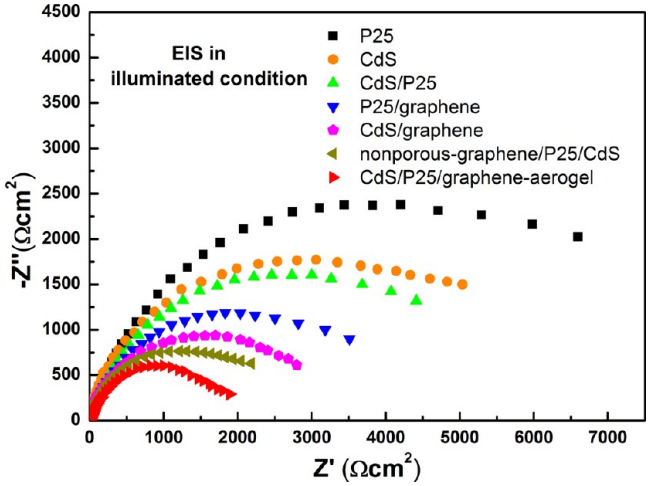

Figure 6. EIS Nynquist plots of CdS/P25/graphene aerogel, nonporous graphene/P25/CdS nanocomposite, CdS/graphene aerogel, P25/graphene aerogel, CdS/P25, CdS nanoparticles, and P25 nanoparticles in a sulfide−sulfite electrolyte and under irradiation of simulated sunlight.

dx.doi.org/10.1021/sc400417u | ACS Sustainable Chem. Eng. 2014, 2, 741−748

In order to explore the photoresponse of the ternary CdS/P25/graphene aerogel, the potentiostatic measurements (current vs time, *I-t*) were performed in the PEC cell containing various catalyst electrodes as photoanodes and Pt as the cathode at 0 V Ag/AgCl under intermittent illumination. Figure 7 exhibits the photocurrent transient responses for the

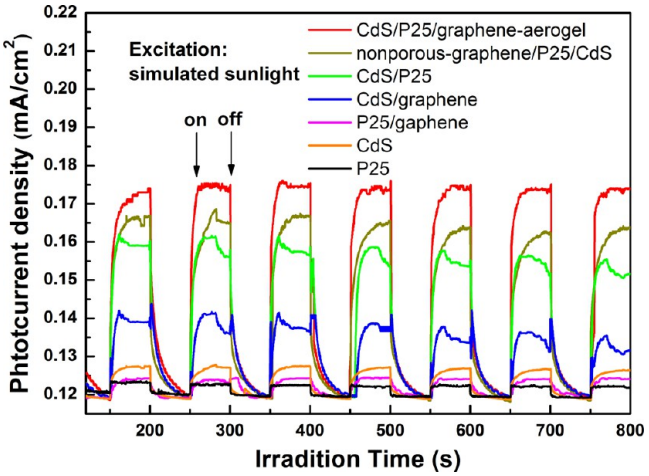

Figure 7. Photocurrent response of CdS/P25/graphene aerogel, nonporous graphene/P25/CdS nanocomposite, CdS/P25, CdS/graphene aerogel, P25/graphene aerogel, CdS nanoparticles, and P25 nanoparticles in a sulfide−sulfite electrolyte with the applied potential of 0 V.

CdS/P25/graphene aerogel, nonporous graphene/P25/CdS nanocomposite, CdS/P25, CdS/graphene aerogel, P25/graphene aerogel, bare P25, and CdS electrodes, respectively. It is noted that there is a fast and uniform photocurrent responding to each switch-on and switch-off event in the CdS/P25/graphene aerogel electrode. Moreover, the photocurrent is so stable that no obvious photocurrent decay is observed. In contrast, the electrodes with the absence of CdS (pure P25 and P25/graphene) exhibit faint but legible photocurrent density, which are much lower than the photocurrent density of the ternary sample, suggesting that the introduction of CdS can be favorable for absorbing visible light. It is interesting that pure CdS behaves with a slight photoresponse, but the presence of P25 (CdS/P25/graphene aerogel and CdS/P25 electrodes) can greatly improve the photocurrent, which is considered to be contributed to the interparticle electron transference between CdS and P25. Furthermore, the photocurrent intensity of the CdS/P25/graphene aerogel is nearly 0.2 mA/cm^2, which is a thousand times more than that of CdS/P25, and the generation of this strong photocurrent is proposed to be the result of the sharp separation of electron−hole pairs with the introduction of graphene. In addition, the stability of the CdS/P25/graphene aerogel has been also evaluated by taking a long-time photoresponse measurement. As shown in Figure 8 (a), during more than 6000 s, only faint photocurrent decay is observed in the primary stage, and the photocurrent density is well maintained even over 60 cycles. Linear scanning voltammograms curves (Figure 8 (b)) of the as-prepared CdS/P25/graphene aerogel electrode after processing 60 cycles (red curve) are also the same as that of the electrode before recycling (black curve). It is illustrated that the construction of the presented ternary aerogel is quite stable in such electrochemical processes, and the function of each component in the hybrid aerogel is also keeping good activity during the photoresponse.

Photocatalytic Mechanism. On the basis of the above analysis, it can be deduced that enhancement of the photocatalytic activity of the ternary CdS/P25/graphene aerogel may be mainly attributed to the following factors: (i) 3D graphene porous architecture with a highly porous ultrafine nanoassembly network structure and excellent electric conductivity and (ii) synergic effects among graphene, CdS, and P25 for reducing the recombination of photogenerated electron−holes pairs. Here, a possible mechanism for the ternary aerogel is proposed, as shown in Figure 9(a,b). In detail, when the system is under sunlight irradiation, both semiconductors CdS and P25 are excited, and the electrons are excited from the valence bands to their conduction bands, thereby forming the photoinduced electron−hole pairs. It is well known that CdS/P25 composite is a type-II band gap alignment, which means the conduction band edge of TiO_2 is located between the conduction band and the valence band of CdS.[42,43] In this band gap structure, a typical interparticle electron transfer process occurs. When electron−hole pairs are generated by sunlight excitation in CdS nanoparticles, the photoelectrons (e^-) can be transferred to the conduction band

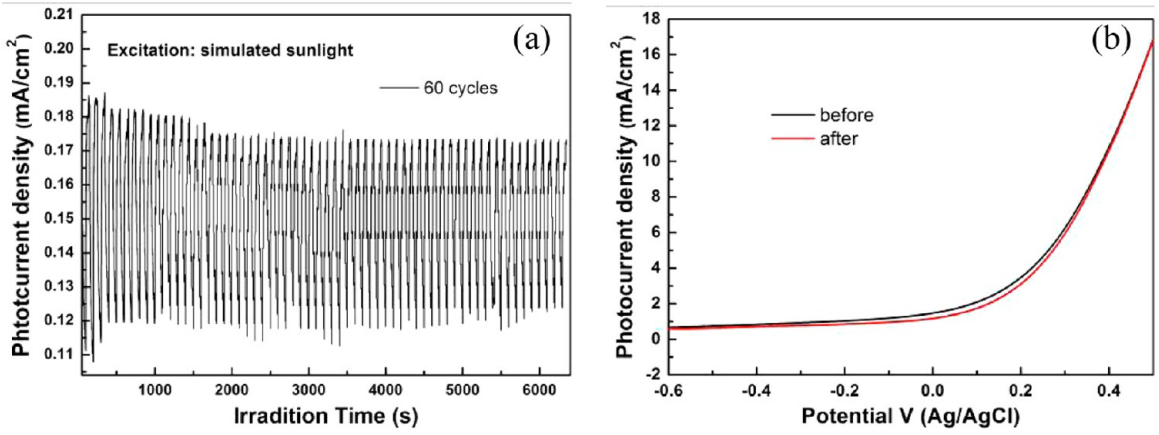

Figure 8. (a) Photocurrent response of CdS/P25/graphene aerogel over 60 cycles obtained in a sulfide−sulfite electrolyte with the applied potential of 0 V. (b) Linear scanning voltammograms curves obtained with CdS/P25/graphene aerogel before recycling (black curve) and after 60 cycles (red curve).

dx.doi.org/10.1021/sc400417u | ACS Sustainable Chem. Eng. 2014, 2, 741−748

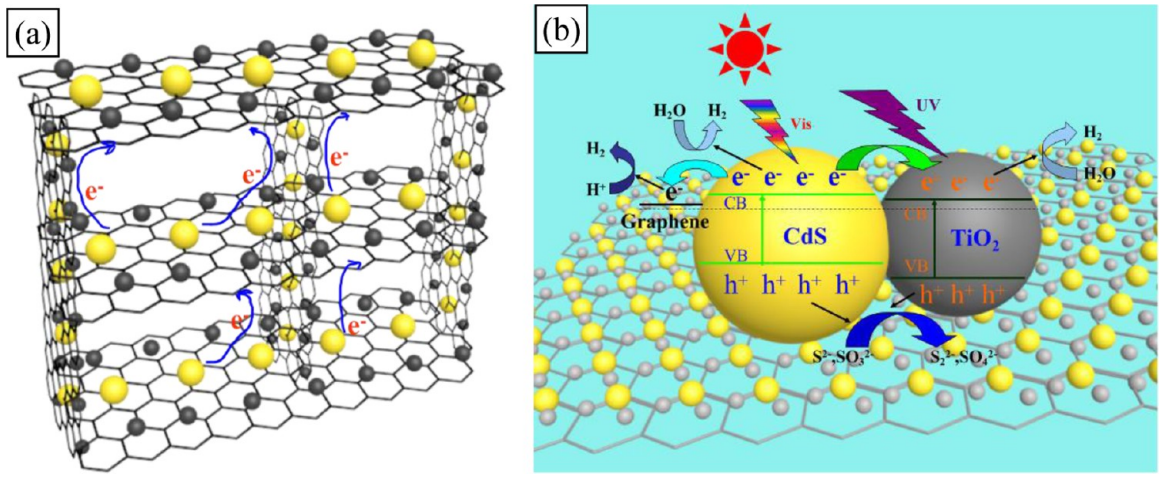

Figure 9. (a) Schematic structure of 3D CdS/P25/graphene aerogel networks. (b) Illustration of the proposed reaction mechanism for hydrogen production over the CdS/P25/graphene aerogel under irradiation of simulated sunlight.

of the TiO_2, which facilitates the charge separation process of electron−hole pairs before they recombine. Simultaneously, partial photogenerated electrons can be transferred from CdS or P25 nanoparticles to the graphene sheets and thus can also prolong the lifetime of the charge carriers. The photogenerated holes (h^+), which remain in CdS, will react with the species in the surrounding electrolyte. Meanwhile, CdS is not stable in aqueous solutions under irradiation due to the anodic dissolution, and such a disadvantage can be avoided in the presence of sacrificial reagents of $S^{2-}$and SO_3^{2-}.[44] In summary, the photogenerated electrons in the CB of CdS can be transferred to TiO_2 through the self-assembled 3D graphene-interconnected network, which acts as a conductive electron transport "highway" and then reacts with the adsorbed H^+ ions to form H_2.

CONCLUSION

In conclusion, we have demonstrated a new strategy by embedding CdS and TiO_2 nanoparticles into an interconnected 3D graphene-based mesoporous microstructure aerogel, which endowed graphene-based materials with large accessible specific surface areas, an interconnected conductive network, and a special microenvironment. Following such motivation, a novel 3D graphene-based CdS/P25/graphene aerogel with high photoelectrochemical performance has been successfully and directly produced by a facile one-step hydrothermal self-assembled approach. We used these CdS/P25/graphene aerogel electrodes in photoelectrochemical studies. The results confirm that the ternary aerogel electrode shows the highest photocurrent, which benefits from superior light-harvesting efficiency, extremely efficient charge separation properties, and superior durability of the material. This work not only demonstrates the potential of 3D graphene as a self-supporting mesoporous microstructure aerogel for embedding nanoparticles in photocatalytic hydrogen production but also highlights more generally the potential applications of graphene-based materials in the field of energy conversion.

ASSOCIATED CONTENT

Supporting Information

Details about the preparation of the comparison groups and working electrodes and some additional figures about the comparison groups. This material is available free of charge via the Internet at http://pubs.acs.org.

AUTHOR INFORMATION

Corresponding Author

*Tel.: +86 0731-58293749. Fax: +86 0731-58298612. E-mail: xqi@xtu.edu.cn.

Author Contributions

†These authors (W. Han and L. Ren) have contributed equally.

Notes

The authors declare no competing financial interest.

ACKNOWLEDGMENTS

This work was supported by grants from the National Natural Science Foundation of China (51002129, 51172191, 11204262, and 11074211), National Basic Research Program of China (2012CB921303), Provincial Natural Science Foundation of Hunan funded support (14JJ3079), Hunan Science and Technology Bureau planned project (2012SK3166), Open Fund based on the innovation platform of Hunan colleges and universities (12K045 and 13K045), Research Fund for the Doctoral Program of Higher Education of China (20124301120006), and China Postdoctoral Science Foundation funded project (20100480068).

REFERENCES

(1) Stankovich, S.; Dikin, D. A.; Dommett, G. H.; Kohlhaas, K. M.; Zimney, E. J.; Stach, E. A.; Piner, R. D.; Nguyen, S. T.; Ruoff, R. S. Graphene-based composite materials. *Nature* **2006**, *442*, 282−6.

(2) Rao, C. N. R.; Sood, A. K.; Subrahmanyam, K. S.; Govindaraj, A. Graphene: The new two-dimensional nanomaterial. *Angew. Chem., Int. Ed.* **2009**, *48*, 7752−7777.

(3) Kamat, P. V. Graphene-based nanoassemblies for energy conversion. *J. Phys. Chem. Lett.* **2011**, *2*, 242−251.

(4) Li, D.; Kaner, R. B. Graphene-based materials. *Science* **2008**, *320*, 1170−1171.

(5) Das, B.; Choudhury, B.; Gomathi, A.; Manna, A. K.; Pati, S. K.; Rao, C. N. R. Interaction of Inorganic Nanoparticles with Graphene. *ChemPhysChem* **2011**, *12*, 937−943.

(6) Dai, L. Functionalization of graphene for efficient energy conversion and storage. *Acc. Chem. Res.* **2012**, *46*, 31−42.

(7) Chen, D.; Zhang, H.; Liu, Y.; Li, J. Graphene and its derivatives for the development of solar cells, photoelectrochemical, and photocatalytic applications. *Energy Environ. Sci.* **2013**, *6*, 1362−1387.

(8) Yu, D.; Nagelli, E.; Du, F.; Dai, L. Metal-free carbon nanomaterials become more active than metal catalysts and last longer. *J. Phys. Chem. Lett.* **2010**, *1*, 2165−2173.
(9) Hu, C.; Cheng, H.; Zhao, Y.; Hu, Y.; Liu, Y.; Dai, L.; Qu, L. Newly-designed complex ternary Pt/PdCu nanoboxes anchored on three-dimensional graphene framework for highly efficient ethanol oxidation. *Adv. Mater.* **2012**, *24*, 5493−5498.
(10) Xu, Y.; Sheng, K.; Li, C.; Shi, G. Self-assembled graphene hydrogel via a one-step hydrothermal process. *ACS Nano* **2010**, *4*, 4324−4330.
(11) Chen, J.; Li, C.; Shi, G. Graphene materials for electrochemical capacitors. *J. Phys. Chem. Lett.* **2013**, *4*, 1244−1253.
(12) Chen, W.; Yan, L. In situ self-assembly of mild chemical reduction graphene for three-dimensional architectures. *Nanoscale* **2011**, *3*, 3132−3137.
(13) Cong, H.-P.; Ren, X.-C.; Wang, P.; Yu, S.-H. Macroscopic multifunctional graphene-based hydrogels and aerogels by a metal ion induced self-assembly process. *ACS Nano* **2012**, *6*, 2693−2703.
(14) Worsley, M. A.; Pauzauskie, P. J.; Olson, T. Y.; Biener, J.; Satcher, J. H.; Baumann, T. F. Synthesis of graphene aerogel with high electrical conductivity. *J. Am. Chem. Soc.* **2010**, *132*, 14067−14069.
(15) Worsley, M. A.; Olson, T. Y.; Lee, J. R. I.; Willey, T. M.; Nielsen, M. H.; Roberts, S. K.; Pauzauskie, P. J.; Biener, J.; Satcher, J. H.; Baumann, T. F. High surface area, sp2-cross-linked three-dimensional graphene monoliths. *J. Phys. Chem. Lett.* **2011**, *2*, 921−925.
(16) Sui, Z.; Zhang, X.; Lei, Y.; Luo, Y. Easy and green synthesis of reduced graphite oxide-based hydrogels. *Carbon* **2011**, *49*, 4314−4321.
(17) Kamat, P. V. Graphene-based nanoarchitectures. anchoring semiconductor and metal nanoparticles on a two-dimensional carbon support. *J. Phys. Chem. Lett.* **2009**, *1*, 520−527.
(18) Chen, W.; Li, S.; Chen, C.; Yan, L. Self-assembly and embedding of nanoparticles by in situ reduced graphene for preparation of a 3D graphene/nanoparticle aerogel. *Adv. Mater.* **2011**, *23*, 5679−5683.
(19) Wu, Z.-S.; Yang, S.; Sun, Y.; Parvez, K.; Feng, X.; Müllen, K. 3D nitrogen-doped graphene aerogel-supported Fe_3O_4 nanoparticles as efficient electrocatalysts for the oxygen reduction reaction. *J. Am. Chem. Soc.* **2012**, *134*, 9082−9085.
(20) Biener, J.; Stadermann, M.; Suss, M.; Worsley, M. A.; Biener, M. M.; Rose, K. A.; Baumann, T. F. Advanced carbon aerogels for energy applications. *Energy Environ. Sci.* **2011**, *4*, 656−667.
(21) Wang, P.; Han, L.; Zhu, C.; Zhai, Y.; Dong, S. Aqueous-phase synthesis of Ag−TiO_2-reduced graphene oxide and Pt−TiO_2-reduced graphene oxide hybrid nanostructures and their catalytic properties. *Nano Res.* **2011**, *4*, 1153−1162.
(22) Ren, L.; Qi, X.; Liu, Y.; Huang, Z.; Wei, X.; Li, J.; Yang, L.; Zhong, J. Upconversion-P25-graphene composite as an advanced sunlight driven photocatalytic hybrid material. *J. Mater. Chem.* **2012**, *22*, 11765−11771.
(23) Lv, T.; Pan, L.; Liu, X.; Lu, T.; Zhu, G.; Sun, Z.; Sun, C. Q. One-step synthesis of CdS−TiO_2-chemically reduced graphene oxide composites via microwave-assisted reaction for visible-light photocatalytic degradation of methyl orange. *Catal. Sci. Technol.* **2012**, *2*, 754−758.
(24) Hoffmann, M. R.; Martin, S. T.; Choi, W.; Bahnemann, D. W. Environmental applications of semiconductor photocatalysis. *Chem. Rev.* **1995**, *95*, 69−96.
(25) Chen, X.; Mao, S. S. Titanium dioxide nanomaterials: Synthesis, properties, modifications, and applications. *Chem. Rev.* **2007**, *107*, 2891−2959.
(26) Kamat, P. V. TiO_2 nanostructures: Recent physical chemistry advances. *J. Phys. Chem. C* **2012**, *116*, 11849−11851.
(27) Zhang, H.; Lv, X.; Li, Y.; Wang, Y.; Li, J. P25-graphene composite as a high performance photocatalyst. *ACS Nano* **2009**, *4*, 380−386.
(28) Zhang, Y.; Pan, C. TiO_2/graphene composite from thermal reaction of graphene oxide and its photocatalytic activity in visible light. *J. Mater. Sci.* **2011**, *46*, 2622−2626.
(29) Kongkanand, A.; Tvrdy, K.; Takechi, K.; Kuno, M.; Kamat, P. V. Quantum dot solar cells. Tuning photoresponse through size and shape control of CdSe−TiO_2 architecture. *J. Am. Chem. Soc.* **2008**, *130*, 4007−4015.
(30) Luo, J.; Ma, L.; He, T.; Ng, C. F.; Wang, S.; Sun, H.; Fan, H. J. TiO_2/(CdS, CdSe, CdSeS) nanorod heterostructures and photoelectrochemical properties. *J. Phys. Chem. C* **2012**, *116*, 11956−11963.
(31) Zhang, N.; Zhang, Y.; Pan, X.; Yang, M.-Q.; Xu, Y.-J. Constructing ternary CdS−graphene−TiO_2 hybrids on the flatland of graphene oxide with enhanced visible-light photoactivity for selective transformation. *J. Phys. Chem. C* **2012**, *116*, 18023−18031.
(32) Hummers, W. S.; Offeman, R. E. Preparation of graphitic oxide. *J. Am. Chem. Soc.* **1958**, *80*, 1339−1339.
(33) Rossetti, R.; Nakahara, S.; Brus, L. E. Quantum size effects in the redox potentials, resonance Raman spectra, and electronic spectra of CdS crystallites in aqueous solution. *J. Chem. Phys.* **1983**, *79*, 1086−1088.
(34) Ohsaka, T.; Izumi, F.; Fujiki, Y. Raman spectrum of anatase, TiO_2. *J. Raman Spectrosc.* **1978**, *7*, 321−324.
(35) Ferrari, A. C.; Basko, D. M. Raman spectroscopy as a versatile tool for studying the properties of graphene. *Nat. Nanotechnol.* **2013**, *8*, 235−246.
(36) Zhang, X.-Y.; Li, H.-P.; Cui, X.-L.; Lin, Y. Graphene/TiO_2 nanocomposites: Synthesis, characterization and application in hydrogen evolution from water photocatalytic splitting. *J. Mater. Chem.* **2010**, *20*, 2801−2806.
(37) Zhang, N.; Zhang, Y.; Pan, X.; Fu, X.; Liu, S.; Xu, Y.-J. Assembly of CdS nanoparticles on the two-dimensional graphene scaffold as visible-light-driven photocatalyst for selective organic transformation under ambient conditions. *J. Phys. Chem. C* **2011**, *115*, 23501−23511.
(38) Sasaki, Y.; Nemoto, H.; Saito, K.; Kudo, A. Solar water splitting using powdered photocatalysts driven by Z-schematic interparticle electron transfer without an electron mediator. *J. Phys. Chem. C* **2009**, *113*, 17536−17542.
(39) Banerjee, S.; Mohapatra, S. K.; Das, P. P.; Misra, M. Synthesis of coupled semiconductor by filling 1D TiO_2 nanotubes with CdS. *Chem. Mater.* **2008**, *20*, 6784−6791.
(40) Wang, D.; Choi, D.; Li, J.; Yang, Z.; Nie, Z.; Kou, R.; Hu, D.; Wang, C.; Saraf, L. V.; Zhang, J.; Aksay, I. A.; Liu, J. Self-assembled TiO_2−graphene hybrid nanostructures for enhanced Li-ion insertion. *ACS Nano* **2009**, *3*, 907−914.
(41) Sun, Y.; Wu, Q.; Shi, G. Graphene based new energy materials. *Energy Environ. Sci.* **2011**, *4*, 1113−1132.
(42) Teranishi, T.; Sakamoto, M. Charge separation in Type-II semiconductor heterodimers. *J. Phys. Chem. Lett.* **2013**, *4*, 2867−2873.
(43) Wang, H.; Wang, T.; Wang, X.; Liu, R.; Wang, B.; Wang, H.; Xu, Y.; Zhang, J.; Duan, J. Double-shelled ZnO/CdSe/CdTe nanocable arrays for photovoltaic applications: microstructure evolution and interfacial energy alignment. *J. Mater. Chem.* **2012**, *22*, 12532−12537.
(44) Emin, S.; Fanetti, M.; Abdi, F. F.; Lisjak, D.; Valant, M.; van de Krol, R.; Dam, B. Photoelectrochemical properties of cadmium chalcogenide-sensitized textured porous zinc oxide plate electrodes. *ACS Appl. Mater. Interfaces* **2013**, *5*, 1113−1121.